Observation and Analysis of Anomalous Terrestrial Diffraction as a Mechanism of Electromagnetic Precursors of Earthquakes

Masafumi Fujii[1*]

[1]Graduate Research Division of Science and Engineering, University of Toyama

Key Points:

- A low-noise high-sensitivity technique is proposed to observe anomalous radio wave signals associated with earthquakes.
- Possible electromagnetic precursors of earthquakes have been detected by observation networks placed near major tectonic lines.
- Large-scale numerical analysis has suggested that anomalous diffraction is the mechanism of the electromagnetic precursors.

*3190 Gofuku Toyama, Japan

Corresponding author: Masafumi Fujii, `mfujii@eng.u-toyama.ac.jp`

Abstract

Detection of earthquake precursors has long been a controversial issue with regard to its possibility and realizability. Here we present the detection of electromagnetic anomalous signals before large earthquakes using an observation network of very high frequency (VHF) radio wave receivers close to major tectonic lines in Japan. The receivers are equipped with specifically designed narrowband filters to suppress noises and to detect extremely weak signals. We detected different types of electromagnetic anomalies before earthquakes around mountainous and coastal regions, where presence of electric charges is anticipated on the surface located in the middle of the radio wave paths near major tectonic lines in Japan. We use numerical electromagnetic wave analysis to show that when electric charges are present on a ground surface as a consequence of tectonic activity, the surface charges interact strongly with radio waves and eventually cause strong diffraction of the radio waves. The analysis was performed using the three-dimensional finite-difference time-domain (3D-FDTD) method with digital elevation models of the actual geographical landforms on a massively parallel supercomputer. The results confirm the consistent mechanisms of the electromagnetic precursors, which explains the anomalous electromagnetic signals observed by the authors before large earthquakes.

1 Introduction

Electromagnetic signals could be enhanced and received at distant locations some days or weeks before earthquakes. Researchers have tried to observe such electromagnetic anomalies and precursors associated with earthquakes for more than 20 years (Kushida & Kushida, 1998, 2002; Fujiwara et al., 2004; Moriya et al., 2005; Hayakawa et al., 2007; Uyeda et al., 2009; Moriya et al., 2009, 2010; Freund, 2011; Yasuda et al., 2009; Bleier et al., 2013). The observation of such anomalies has been difficult and unstable because they are affected by geographical, atmospheric, ionospheric conditions and disturbed by environmental noise of random nature. Various possible electromagnetic precursors have been so far reported and a number of hypotheses have been proposed: i.e., ionospheric perturbation by Kushida et al. (Kushida & Kushida, 1998, 2002) and Hayakawa et al. (Hayakawa et al., 2007; Yasuda et al., 2009; Bleier et al., 2013), lithosphere-atmosphere-ionosphere (LAI) coupling by Pilipenko et al. (Pilipenko et al., 2001), atmospheric anomalies (Fujiwara et al., 2004), a bulk plasmon model (Kamogawa & Ohtsuki, 1999), and chemical models (Enomoto & Hashimoto, 1990; Enomoto et al., 1997). All of these models are inclusively possible, not exclusively, but difficult to explain the anomalous radio wave phenomena comprehensively, especially in the very high frequency (VHF) band.

On the other hand, the mechanism of the anomalous radiowave propagation has been explained reasonably by the theory of the ground surface plasma wave appearing on the surface of the Earth (Fujii, 2013, 2016). It has been experimentally shown that positive electric charge carriers come out from the peroxy bond in oxidized minerals when rocks are subjected to tectonic deviatoric stresses (Freund, 2000, 2002, 2011; Bleier et al., 2013), and that such carriers can even move across the composite boundary of rocks along crustal faults. Although it is still controversial, this fact could explain the possible presence of electrostatic charges on the Earth's surface associated with co-seismic or pre-seismic activities. Another possibility is the change of ground resistivity with earthquakes (Rikitake & Yamazaki, 1978) even at a distance of 1,000 km from epicenters, which could be supported by the theory that the size of the precursor deformation zone of earthquakes is estimated by a simple formula as a function of its magnitude (Dobrovolsky et al., 1979). Therefore, electric charges on the ground surface must play a role in seismic activity. In general, if electric charges exist on a surface, then the charges are subjected to the force by the external oscillating electric field. This is equivalent to the well-known surface plasmon in optics induced by light on metal surfaces (Kittel, 1986; Raether, 1977, 1988; Fujii, 2014).

In this paper, we present our observation results of anomalous radio wave signals that strongly depend on the polarization and the propagation path of the wave. We then analyze the propagation of the radio waves and show a possible mechanism of the anomalous propagation and diffraction caused by an interaction between the radio wave and the surface electric charges, which can be referred to as the terrestrial surface plasmon. This paper does not deal with the fundamental mechanism of the earthquake itself, but rather focuses on the possible electromagnetic phenomena on the Earth's surface with electric charges associated with earthquakes. The analysis was performed using the three-dimensional finite-difference time-domain (3D-FDTD) method (Yee, 1966; Taflove, 1995) with the properties of the mobile electric charge carriers of the Drude dispersion model (Taflove & Hagness, 2005; Fujii, 2013, 2016). The analysis method and the computational code have been verified by comparison with the theoretical solutions of localized surface plasmons on a metal sphere (Fujii, 2014). Several analyses have been carried out with different landforms of irregular shapes in mountainous regions and coasts to show that the electromagnetic interactions occur randomly and depend strongly on the topography of the ground surface. The numerical results agree well with the observed polarized radio wave signals.

2 Radio Wave Observation Geometry and Equipment

We observe radio waves from distant broadcast stations as shown in Figure 1 and in Table 1. Since these radio signals are significantly weak, we have developed highly sensitive low-noise measurement systems that employ super-narrow-band filters for significant noise reduction implemented over a network of distant observation sites (Fujii, 2023a).

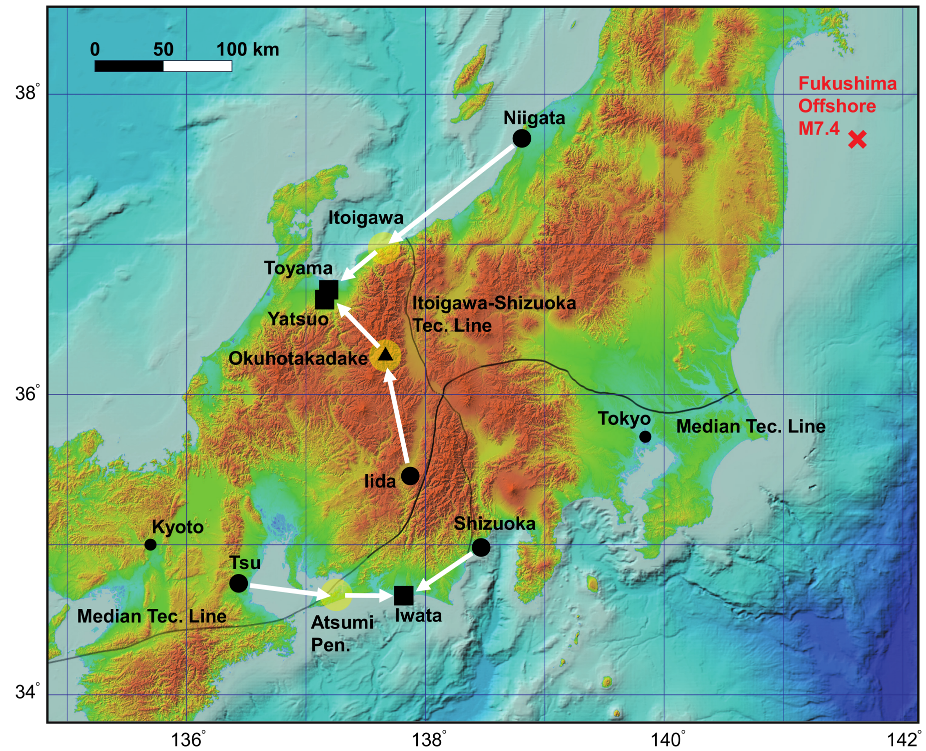

Figure 1. The map of broadcast and observation stations focused in this study as listed in Table 1 and the epicenter of the $M7.4$ Fukushima offshore earthquake (E141° 37'22", N37° 41'48", depth 57 km) on Mar. 16, 2022 at 23:36:32.6 (JST) on the Pacific side of Japan. The symbols of the black circle and the square are for the broadcast and observation stations, respectively. White arrows indicate the radio wave paths, and the yellow circular regions indicate the possible points of causing anomalous diffraction, which are Mt. Okuhotakadake, Atsumi Peninsula, and Itoigawa, analyzed in the following sections. Thin black lines are the Median Tectonic Line and the Itoigawa-Shizuoka Tectonic Line. Tokyo and Kyoto are shown for reference. The earthquakes in the Kamikochi/Okuhotakadake region discussed later and listed in Table 2 occurred in the limited area within approximately 10 km distance of the black triangle near the center of the map.

2.1 Noise Reduction by Super-Narrow-band Notch Filter and Observation System

The radio wave observation system is composed of standard Yagi antennas of 3 to 6 elements in horizontal and/or vertical polarization depending on the allowable facility as summarized in Table 1, and digital radio receivers AOR AR5001D and/or AR2300, which are controlled by PCs. The radio wave is measured every 10 s at the Toyama and Yatsuo stations, and every 20 s at the Iwata station. For stable detec-

Table 1. List of the radio broadcast and observation sites focused in this paper. The polarization and the number of elements of the Yagi antennas at the observation sites are shown in parentheses with the form of (Polarization, Number of elements). Polarization notations H and V are for horizontal and vertical linear polarizations, respectively. Height is that of antenna comprised of altitude above sea level and approximate height of antenna facility. 80.9 MHz is an unused frequency in Japan and is monitored for comparison as discussed in the text.

Observation sites: Site Name	(Pol., Elem.)	Longitude	Latitude	Height (m)
For Toyama/Yatsuo:				
Toyama City, Toyama Pref.	(H,5) (V,6)	E137° 11'13"	N36° 41'38"	30
Yatsuo, Toyama City, Toyama Pref.	(H,3)	E137° 07'51"	N36° 37'10"	30
For Iwata:				
Iwata City, Shizuoka Pref.	(H,5)	E137° 49'20"	N34° 39'20"	4

Broadcast sites: Freq.(MHz)	Power	Site Name	Pol.	Longitude	Latitude	Height (m)
For Toyama/Yatsuo:						
80.9	0 W	(no broadcast)	–	———	———	—
82.3	1 kW	Niigata	H	E138° 48'30"	N37° 42'24"	600
88.3	100W	Iida	H	E137° 52'21"	N35° 27'33"	771
For Iwata:						
78.9	3 kW	Tsu	H	E136° 26'01"	N34° 43'57"	320
79.2	1 kW	Shizuoka	H	E138° 27'56"	N34° 58'27"	300
80.9	0 W	(no broadcast)	–	———	———	—

tion of earthquake precursors, effective noise reduction in the measurement system is essential. Super-narrow-band notch (band-rejection) filters (Fujii, 2021) are inserted between the antenna and the receiver to reduce unwanted intense radio waves from nearby broadcast stations by more than 20 dB from a typical −50 dBm signal level down to −70 dBm, etc., allowing clear uninterrupted observation even in urban areas as described in the following. Note that dBm is a unit of electric power in dB relative to 1 mW reference power.

The frequency characteristics of the super-narrow-band notch filter used for the Toyama observation station are shown in Figure 2 (a). The filter attenuates the radio wave signals from nearby stations by −25 dB each, and the rejection bandwidth is as narrow as approximately 1 MHz. Since the target signal from the Niigata broadcast station at 82.3 MHz is very close to the unwanted signal at 82.7 MHz, the target signal is also attenuated by approximately −11 dB; this may unwillingly degrade the necessary radio wave power. However, the third-order intermodulation caused in the amplifying circuit of most receivers would have worse effects, which has been reduced by the filters by more than −30 dB. This results in the reduction of the noise floor under −90 dBm to −100 dBm as shown in Figure 2 (b).

Note that 80.9 MHz is a frequency that is not used for broadcasting in Japan; it is monitored in this study to see if broadband noise is observed simultaneously with anomalous signals at different frequencies (Yoshida et al., 2006). The effect of the filter is clearly seen when the filter was removed occasionally for maintenance on March 9, 2022, from 12:00 to 17:00, and the noise floor increased by 30 dB to 40 dB depending on the frequency due to the nonlinear intermodulation effect. The reduction of the third-order intermodulation noise is therefore considered critical and has a higher priority than the slight loss of necessary signals; otherwise, the precursors are weak and hidden behind the noise. Note also that different filters and receiver are used for each observation system, even at the same site, depending on the directions of the target broadcast stations. The 88.3 MHz wave from Iida is observed with a different system than the 82.3 MHz wave from Niigata, and therefore it is not shown in Figure 2, whereas the noise reduction capability is in the same level.

The super-narrow-band notch filter consists of a series capacitor of several pico-farads and a high quality-factor (low-loss) inductance of approximately 1 nH. The inductance is formed by a short-circuited low-loss 12D-FB coaxial cable of 60 cm to 70 cm length, determined according to the frequency to be rejected, and has a quality-factor of 25 to 30 at the VHF band. The circuit is shown in Figure 2 (c) for one unit structure; for its use in actual observation, a necessary number of the unit structures are cascaded as shown in Figure 2 (d). It should be noted that commercially available inductors are mostly not applicable due to their much higher losses and lower quality factors.

The notch filters are used in all observation systems to attenuate unwanted radio wave signals and reduce the noise floor; thus, it is not necessary to go to an unpopulated district in search of an electromagnetically quiet environment for observation. In addition, the coaxial cables connecting the antennas and receivers are loaded with numerous ferrite cores to reduce the common-mode noise. The target broadcast stations were chosen in such a way that their radio signals were significantly weak but close to the limit of detection. The system was first operated for a certain period of time to search for radio waves that carry anomalies under critical propagation conditions.

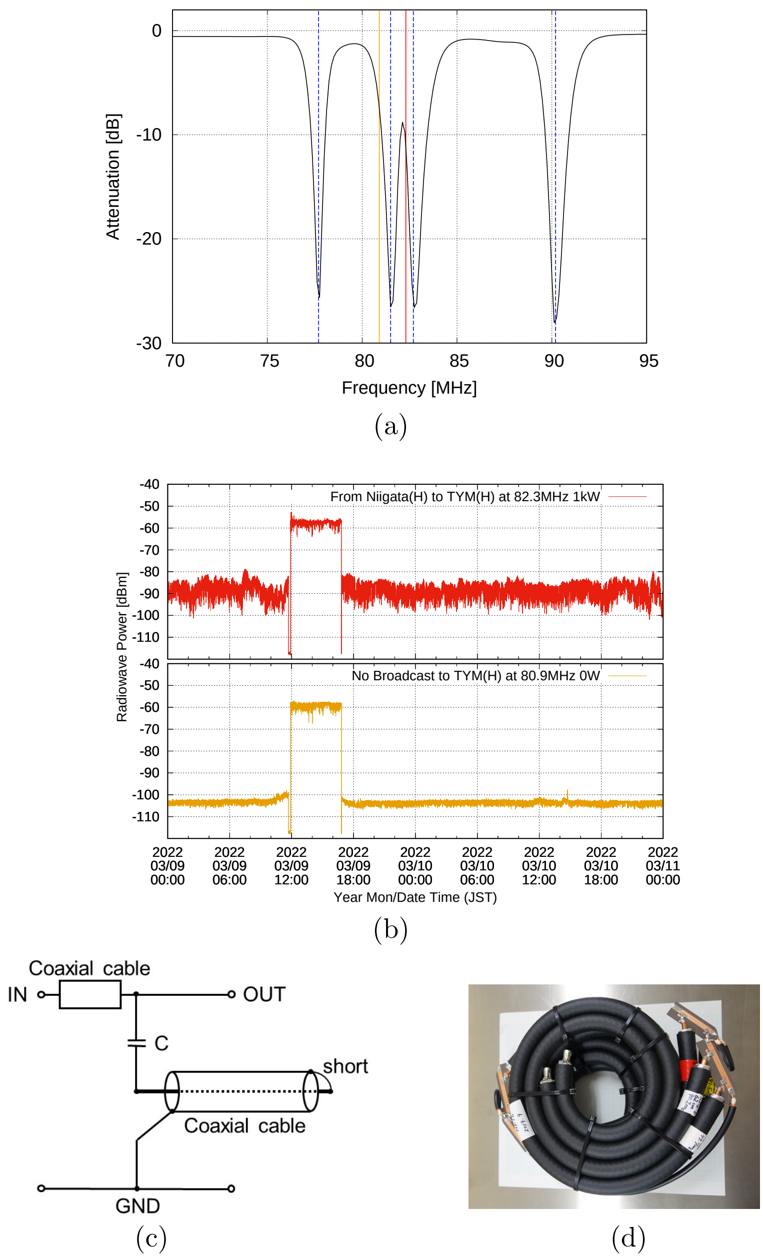

Figure 2. An example of the super-narrow-band notch filter implemented in one of the observation systems in Toyama. (a) Frequency characteristics of the whole filter. Blue dotted lines show the frequencies to be rejected i.e., 77.7 MHz, 81.5 MHz, 82.7 MHz, and 90.2 MHz for the Toyama station (TYM), and the orange and red solid lines show the target frequencies to be observed at 80.9 MHz and 82.3 MHz, respectively. (88.3 MHz wave from Iida is observed by another system and is therefore not shown here.) (b) Noise reduction effect of the filter; the filter was removed for occasional maintenance on March 9th from 12:00 to 17:00, i.e., for the period of the high-level state of the step, otherwise the filter was inserted. The height of the step is, therefore, the level of the achieved noise reduction. "(H)" refers to the antenna polarization as horizontal. (c) Unit circuit of the notch filter. (d) The appearance of the whole filter. A total of 8 units are cascaded to reject 4 frequencies. The coaxial cables are rolled to fit in a 25 cm-wide, 30 cm-long, and 10 cm-high box.

3 Observed Anomalous Radio Signals before Earthquakes and Numerical Analysis

In this paper, we show first some of the anomalous signals that we observed by the above-mentioned system. In order to clarify the physical mechanism of the anomalous radio wave propagation that is possibly related to earthquakes, we have performed large-scale electromagnetic analyses using the FDTD method on a massively-parallel supercomputer with digital elevation models of the landforms. We have analyzed the effect of landforms such as mountains, valleys, and coasts, with and without electric charge carriers on the propagation of electromagnetic waves in air and on surfaces (Fujii, 2013, 2016, 2023b, 2024c). The computational resources used for the analyses were 64 nodes, 2304 CPU cores, 3 to 5 TB of memory, and the wall time of 5 to 20 hours per job on a Cray CS400 supercomputer.

3.1 Mountainous Region of Japan Alps

In the region of Japan Alps, we had a series of earthquakes larger than $M5$ in April - May, 2020, as listed in Table 2, near the Okuhotakadake peak (E137° 38'53", N36° 17'20", height 3189.5 m), referred also to as Kamikochi region shown near the center of Figure 1. Since approximately a year before the earthquakes, we observed a series of anomalous signals; in the normal state, the signal level was below -100 dBm, but suddenly it increased by about 20 dB and lasted for several hours or even longer and returned to the previous signal level; they look like rectangular pulses with different periods and heights, as shown by the arrows in Figure 3. A single rectangular pulse signal was observed on December 30, 2016, as shown in Figure 3 (a), which may be due to the possibility that the preparation phase of the earthquakes continues intermittently, as earthquakes occur periodically in this particular region, including the group of small events in 2018; the origin of this single anomaly has not yet been identified.

Similar phenomena of such pulse anomalies have also been observed regarding the pre-seismic radio wave propagation, and its statistical analysis was presented for earthquakes in a mountainous area in Hokkaido, Japan (Moriya et al., 2010). In the case of our observations, an association with earthquakes can also be inferred. In Figure 3(a), the times of the earthquakes are indicated by the stars. Interestingly, these anomalous signals appear mostly in the vertical polarization (upper plots) and not in the horizontal polarization (lower plots), while the polarization of the broadcast radio wave is horizontal, which is difficult to explain by artificial noise and can be presumed to be a natural phenomenon. More detailed anomalous signals for this case are shown in Supporting Information (Fujii, 2024c) Section 3.1 Figures 27 to 29.

From these facts, it is presumed that the radio wave from Iida is diffracted by the high peaks of the Japan Alps and then reaches the observation station in Toyama. This propagation path is obviously out of sight due to the high mountains in this region. However, it is an interesting problem how radio waves propagate when electric charges appear on the surface of the mountain peaks, which has been studied by the numerical analysis in the following.

3.1.1 Numerical Analysis Conditions

As shown in Figure 4, the size of the analysis region is chosen to be 860 m from west to east, 710 m from south to north including the peak point at the origin of the analysis region, and an altitude higher than 3070 m up to 3240 m i.e., 170 m in height. The peak of the mountain has an altitude of 3189.5 m, and the gap between the peak and the upper boundary of the analysis region is approximately 50 m. The original digital elevation model (DEM) grid has a resolution of about 5m, and finer

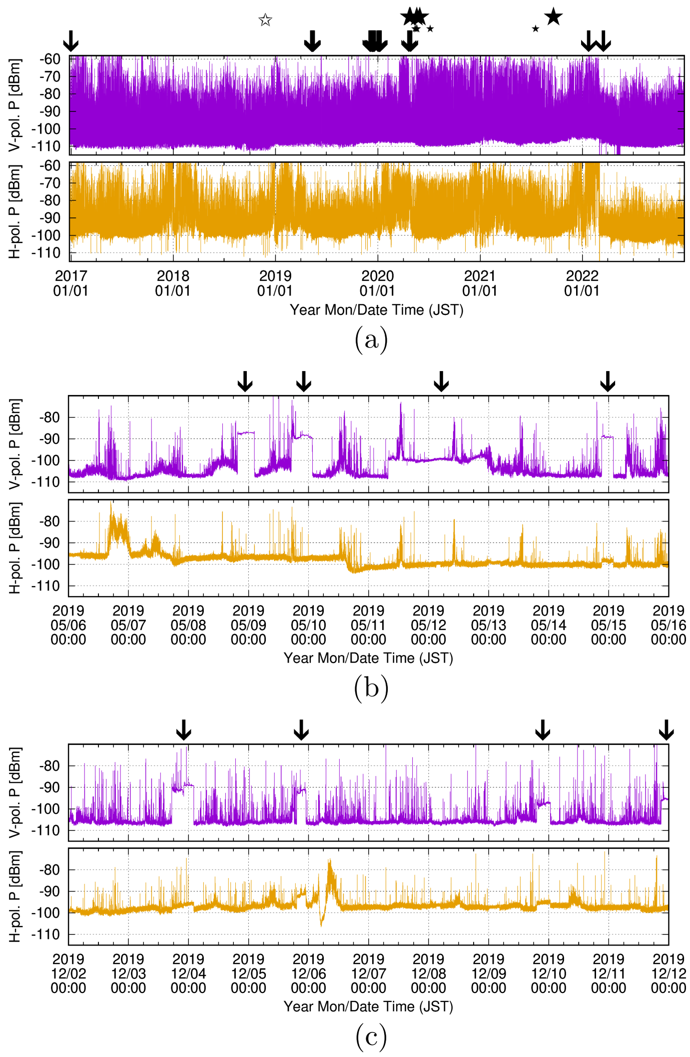

Figure 3. (a) Observed radio wave power in dBm for the wave propagation from Iida to Toyama at 88.3MHz since 2017 till 2022 obtained by the authors; time data for the whole observation period are plotted to show their long-term perspective. For more detailed signals, see (b) and (c), and their descriptions below. Arrows indicate the time of occurrence of the anomalous rectangular-shaped pulse signals. Large black stars indicate the time of the major earthquakes in Kamikochi district ranging from $M5$ to $M5.5$ (JMA); some of which occurred in a particular short period are listed in Table. 2. Small black stars show those of smaller earthquakes of $M4.3$ to $M4.8$ in the same district. A medium white star shows a group of 49 small earthquakes of $M1.9$ to $M3.1$ in the same district during the short period from November 23 to November 30, 2018. After these major events, anomalous rectangular-shaped signals are rarely seen, except for short ones lasting less than a few minutes. (b) Example of the observed signals expanded for 10 days from May 6 to May 16, 2019. (c) Another example of the period of 10 days from Dec. 2 to Dec. 12, 2019. The anomalous rectangular-shaped pulses with sudden increase in their power levels are pointed by the arrows in (b) and (c). For each sub-figure, the upper plot is the vertical polarization data and the lower plot is the horizontal polarization data. The anomalous rectangular signals are mostly observed for the vertical polarization. The data for the horizontal polarization exhibit some spike noises and those possibly caused by sporadic E layers in ionosphere, and some very weak rectangular anomalies are seen at the same time as those for the vertical polarization.

Table 2. List of the major earthquakes in the Kamikochi/Okuhotakadake district discussed in this section. They occurred in a limited area of approximately 10 km distance near the center of Figure 1 (black triangle), and within a time period of about a month. Magnitude M is of JMA. The maximum seismic intensity of Japan scale (Max SI) is also shown.

No.	Epicenter (Longi. Lati.)	M	Date	Time (JST)	depth	Max SI
1	Nagano middle part E137° 39'42" N 36° 13'30"	5.5	April 23, 2020	13:44:22.1	3 km	4
2	Nagano middle part E137° 39'00" N 36° 14'06"	5.0	April 23, 2020	13:57:55.1	5 km	3
3	Nagano middle part E137° 38'12" N 36° 15'06"	5.0	April 26, 2020	02:22:49.4	6 km	3
4	Gifu Hida District E137° 37'42" N 36° 17'00"	5.4	May 19, 2020	13:12:58.1	7 km	4
5	Nagano middle part E137° 38'24" N 36° 15'42"	5.3	May 29, 2020	19:05:14.9	4 km	4

grids of 0.2 m resolution were obtained by spline interpolation for the FDTD analysis. The boundaries of the analysis region were all set to be the perfectly matched layer (PML) absorbing boundary of 50 layers and the reflection from the boundary was minimized. For the whole mountain model, the relative dielectric permittivity was set to $\epsilon_\infty = 6$ and the electric conductivity $\sigma = 1.0 \times 10^{-3}$ S/m. The parameters of the Drude dispersion are plasma frequency $f'_p = 408$ MHz and damping frequency $\Gamma = 2\pi \times 10^7$ rad/s for the electrically charged ground (Fujii, 2016). The incident wave has horizontal polarization of the E_z component, same as the real radio broadcast, and the frequency is set to be 70 MHz i.e. the wavelength is 4.3 m in air. The incident wave is entered in the x-direction from south to north so that it hits the peak of the mountain.

3.1.2 Numerical Results

The analysis results are shown in Figure 5. To distinguish the behavior of radio waves for the cases with and without the surface charges, it is easily recognizable to plot only the vertical component E_y. The vertical cross-section of the landform on which the radio wave field will be plotted is shown in Figure 5(a). In these plots, the incident wave is not included; only the scattered or diffracted wave in the vertical polarization is observed. In the case where no earthquake is expected and there is no surface electric charge, the radio wave is diffracted at the peak as a normal phenomenon and the wave partially penetrates the ground as shown in Figure 5(b). In contrast, for the case where crusts are stressed and electric surface charges appear on the peak, the radio wave is strongly scattered and diffracted in random directions as shown in Figure 5(c); this is considered to be the anomalous mountain diffraction caused by the peak covered with surface electric charges.

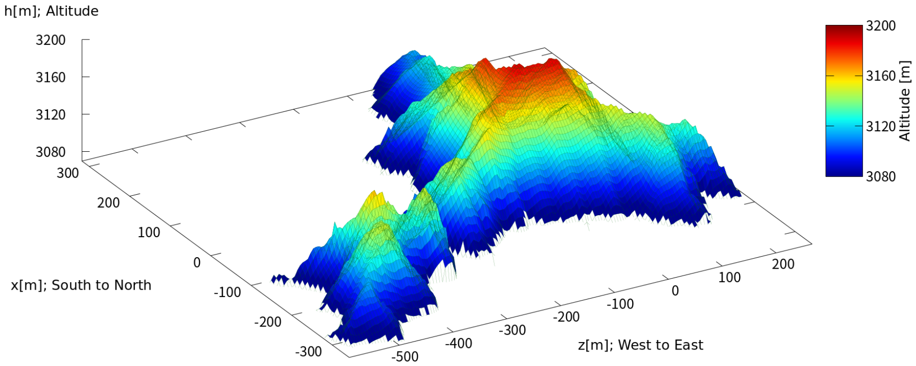

Figure 4. 3D model of the Okuhotakadake peak of 3189.5 m altitude. The origin of the horizontal axes is collocated with the peak. Altitude h is taken in the y-direction. The digital elevation model (DEM) is publicized by the Geographical Survey Institute, Japan.

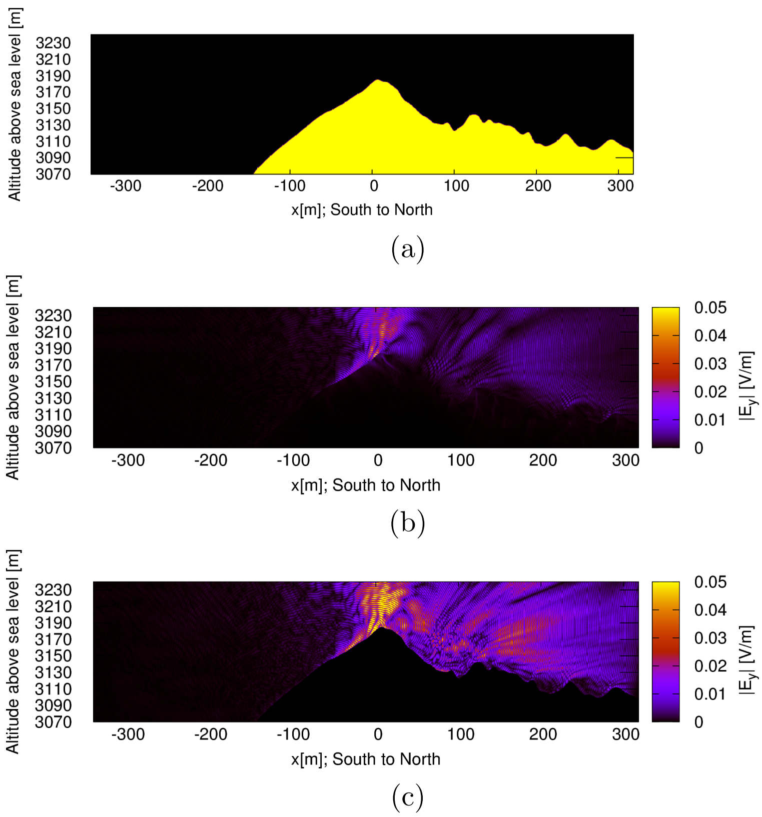

Figure 5. FDTD analysis results of the vertical component $|E_y|$ for the Okuhotakadake peak on the vertical plane from the south to the north that includes the peak point. The incident wave is of horizontal E_z polarization. Altitude h is taken in the y-direction. (a) Vertical landform on the plane of the field plot, (b) without surface charge, and (c) with surface charge.

In Figure 6, similar effects are clearly observed in the horizontal plane at 3120 m. These results clearly show that the radio wave strongly interacts with the surface electric charges; the strong field along the surface is considered to be the surface plasma wave or the surface plasmon and they are induced around the peak and propagate downward along the surface. They are partly scattered by surface roughness and re-radiate the radio waves, which are diffracted again by the next lower peaks. Interestingly, the radio wave is scattered toward various random directions in a beam-like form as clearly seen in Figure 6(c) compared to (b). This randomness in the scattering and diffraction would cause the randomness in the ability to detect the anomalous signals at particular observation locations, i.e., anomalies are detectable in some locations, but not in others, literally randomly, as the electric charges on the ground surface vary according to the stress to the crusts. The beam-like diffraction is a general phenomenon that is commonly seen in most of our analyses; this could be a possible mechanism for an anti-symmetric behavior of the observation results in Toyama and in Yatsuo, as discussed in the next section.

It is of particular importance to evaluate the quantitative agreement between the observation and the numerical analysis. We assume the typical environmental conditions for a broadcast radio wave with its source power P_0 =1 kW, and it is observed at a distance of r =100 km. Then, the intensity (magnitude of the pointing vector or the power flow per unit area) of the radio wave is estimated over a tentative sphere surface of radius r as $p = P_0/4\pi r^2 \approx 8 \times 10^{-9}\,\mathrm{W/m^2}$. In the numerical analysis, the electric field strength of the incident wave is set to approximately 1 V/m, and that of the diffracted radio wave is typically 1 % to 5 % of the incident wave that is found in Figures 5 and 6. If we assume that it is 1 %, then the intensity of the diffracted wave will be $p = 8 \times 10^{-9} \times 0.01^2 = 8 \times 10^{-13}\,\mathrm{W/m^2} = 8 \times 10^{-10}\,\mathrm{mW/m^2}$ (milli-watts per square meter). We also assume that the effective antenna cross section for the Yagi antenna is of the order of $a = 1\,\mathrm{m^2}$, then, the received power for the Yagi antenna is estimated to be $P = a\,p = 8 \times 10^{-10}\,\mathrm{mW}$, which is $10 \log_{10} P \approx -90\,\mathrm{dBm}$; this value is the receivable power when the anomalous diffraction occurs, and is consistent with the received power for the observed anomalous signals, typically -90 dBm to -100 dBm as found in all the observation results such as Figure 3, and Figure 7 in the later section.

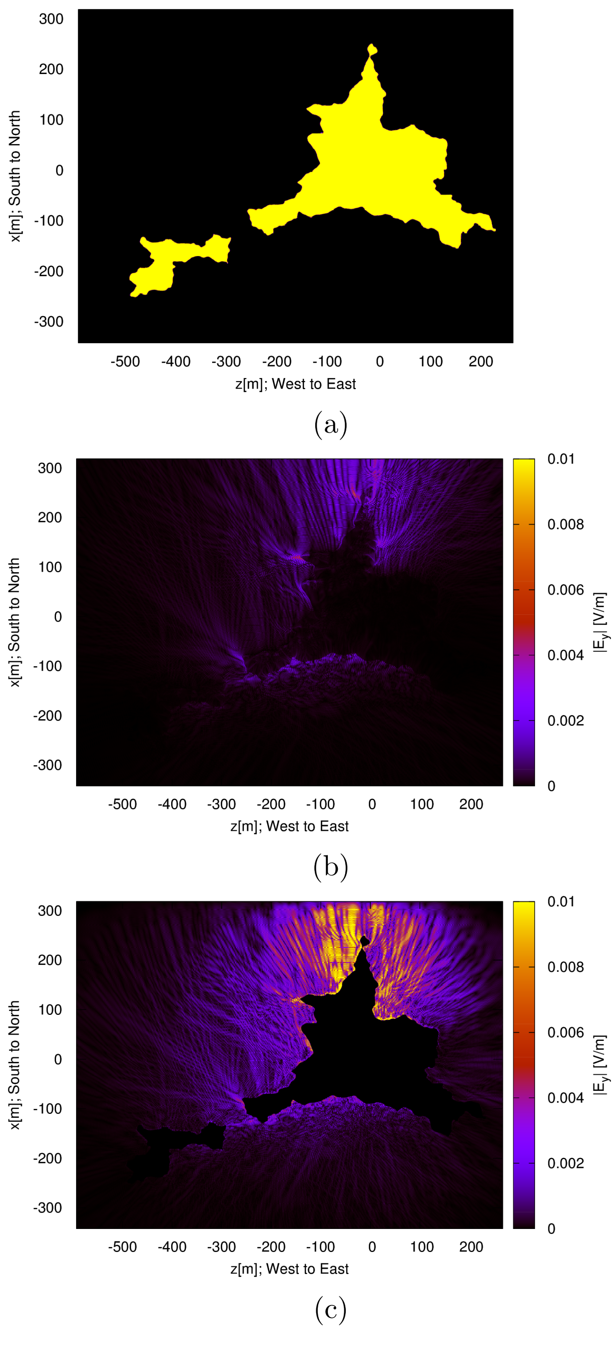

Figure 6. FDTD analysis results of vertical component $|E_y|$ for the Okuhotakadake peak on the horizontal plane at an altitude of 3120 m, which is 69.5 m down from the peak. The incident wave is of horizontal E_z polarization incoming from the south. (a) Configuration of the landform on the plane of the field plot, (b) without surface charge, and (c) with surface charge.

3.2 Pacific Coast of Central Japan

Next, we consider the anomalous radio wave propagation in the coastal regions. As shown in Figure 7, one day before the Fukushima earthquake of $M7.4$ on March 16, 2022, we detected significantly clear radio wave signals of possible earthquake precursors at two locations over 200 km apart (Fujii, 2023a). For this event, the anomalous signal at the Iwata observation station from the Tsu broadcast station (fourth slot from above) was much larger than those at the Toyama (first slot) and Yatsuo (second slot) stations, leading to the implication of earthquakes occurring near the Pacific side rather than the Japan Sea (north) side. Eventually, about 15 hours after the maximum of the anomalous signal, the Fukushima offshore earthquake occurred. The epicenter for this event is shown in Figure 1. The anomalous signal from the Shizuoka broadcast station to the Iwata observation station (third slot in Figure 7) also exhibits moderate variation, which could be due to the influence of the nearby Itoigawa-Shizuoka Tectonic Line. More examples of the anomalous signals are found in Supporting Information (Fujii, 2024c) Sections 4.2.3 and 4.2.5.

It is very interesting to note that the variation of the anomalous signals for Toyama (first slot) and Yatsuo (second slot) shows an anti-symmetric behavior; when the signal increases in Toyama, the signal decreases in Yatsuo, and vice versa. Such phenomena in a small district of only 10 km distance is difficult to explain by meteorological or ionospheric phenomena such as radio ducting and sporadic E layers, but can be explained by anomalous diffraction due to surface electric charges as discussed in the previous section; more details are found in (Fujii, 2024c) Section 4.2.4.

Note also that, in Figure 7, the observed signals show some smaller fluctuations even after the main shock (e.g. March 17, 2022, at 00:00 in the second slot, and same day at 8:00 in the fourth slot, also smaller fluctuations in other plots). These post-cursor signals are often seen in other cases as well, which can be attributed to the crustal activity in the associated nearby regions, and to the other smaller earthquakes. More examples are found in (Fujii, 2024c) Section 4.2.7. Although there are some uncertainties that are difficult to fully describe, the significance in this case is that the major anomalies occurred almost simultaneously. Long-term observation data are found again in (Fujii, 2024c) Section 4.2.6 and in Supporting Data Set-1 and 2 (Fujii, 2024a, 2024b) on the corresponding pages in chronological order. It is also noteworthy that during the period of the Fukushima $M7.4$ earthquake in Figure 7, 80.9 MHz signals did not show any particular variations either in Toyama, Yatsuo or in Iwata observation station, suggesting that no broadband noise was observed; for the observation data, see (Fujii, 2024c) Section 4.2.3 Figures 6 to 9, and related part.

3.2.1 Numerical Analysis Conditions

In the lower part of Figure 1, the landform near the radio wave path from Tsu to Iwata is shown by white arrows. Along this radio wave path, there are some landforms that can cause radio wave diffraction, such as high cliffs along the Pacific coast of Atsumi peninsula. The numerical model of the coast including the cliff of several ten meters in height is shown in Figure 8. The size of the analysis region is 1420 m from west to east, 600 m from south to north, including a part of the Pacific Ocean. The total height of the analysis region is 100 m; the height above sea level is 96 m, added with the tentative 2 m-deep sea water and 2 m-thick sea bottom, which have little effect on the analysis results.

The relative dielectric permittivity was set to $\epsilon_\infty = 6$ and the electrical conductivity $\sigma = 1.0 \times 10^{-3}$ S/m for the ground, and $\epsilon_\infty = 80$, $\sigma = 4.0$ S/m for the seawater.

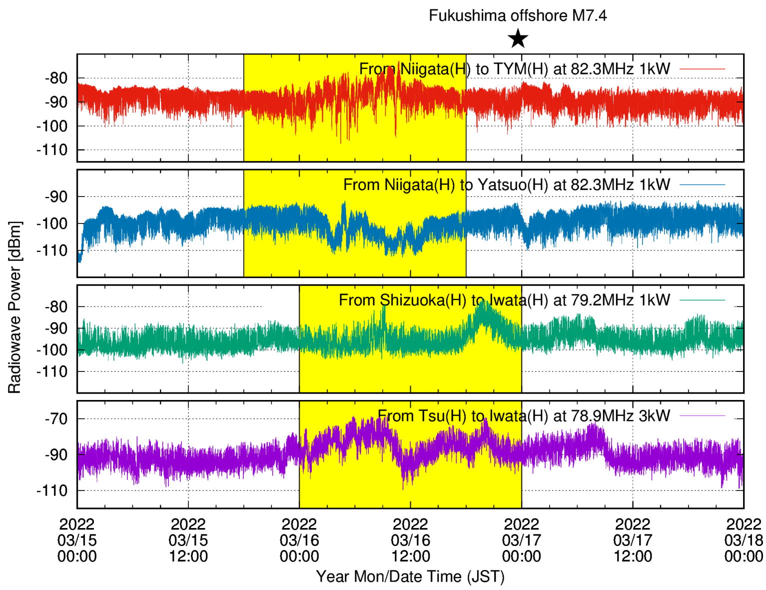

Figure 7. Comparison of the anomalous signals observed in Toyama, Yatsuo and Iwata around the Fukushima offshore $M7.4$ earthquake on March 16, 2022. Star symbol shows the time of the earthquake.

The parameters of the Drude dispersion are $f'_p = 408\,\mathrm{MHz}$ and $\Gamma = 2\pi \times 10^7\,\mathrm{rad/s}$ for the electrically charged ground as in the previous analysis. The seawater was treated as a normal lossy conductive medium. The grid size of the DEM is approximately 5 m, and it was refined by the spline interpolation to obtain the FDTD grid of 0.2 m resolution. The analysis region is surrounded by 50 layers of perfectly matched layer (PML) absorbing boundaries and was analyzed with the 70 MHz incident radio wave from the west.

3.2.2 Numerical Results

In the analysis results, for the case where electric charges are present on the surface, it was found that polarization-dependent anomalous diffraction of radio waves can occur (Fujii, 2023b), which is shown in Figure 9; due to the complicated landform, the scattered and diffracted radio waves form many narrow beams and radiate in random directions, which is clearly seen in (c) compared to the result in (b). In particular, due to the high cliff that runs for long distance along the Pacific coast, it is presumed that horizontally polarized waves are scattered and diffracted, which are all superimposed, and the enhanced wave reaches the observation site. These results suggest the physical mechanism of the anomalous radio wave signals caused by the interaction between the surface charges and radio waves.

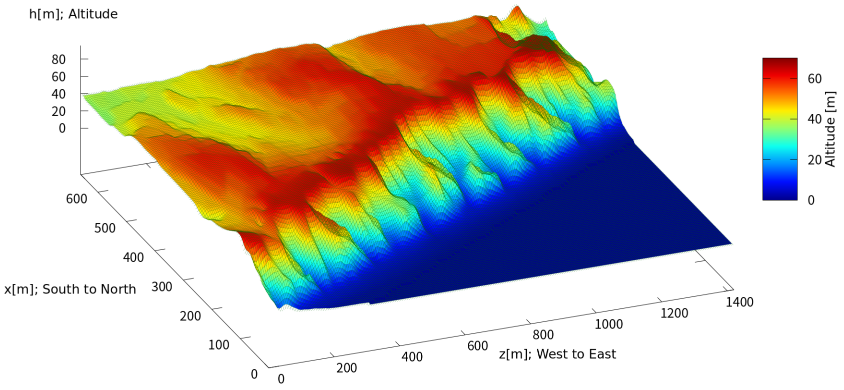

Figure 8. The 3D analysis configuration of a south coastline of Atsumi Peninsula indicated in Figure 1.

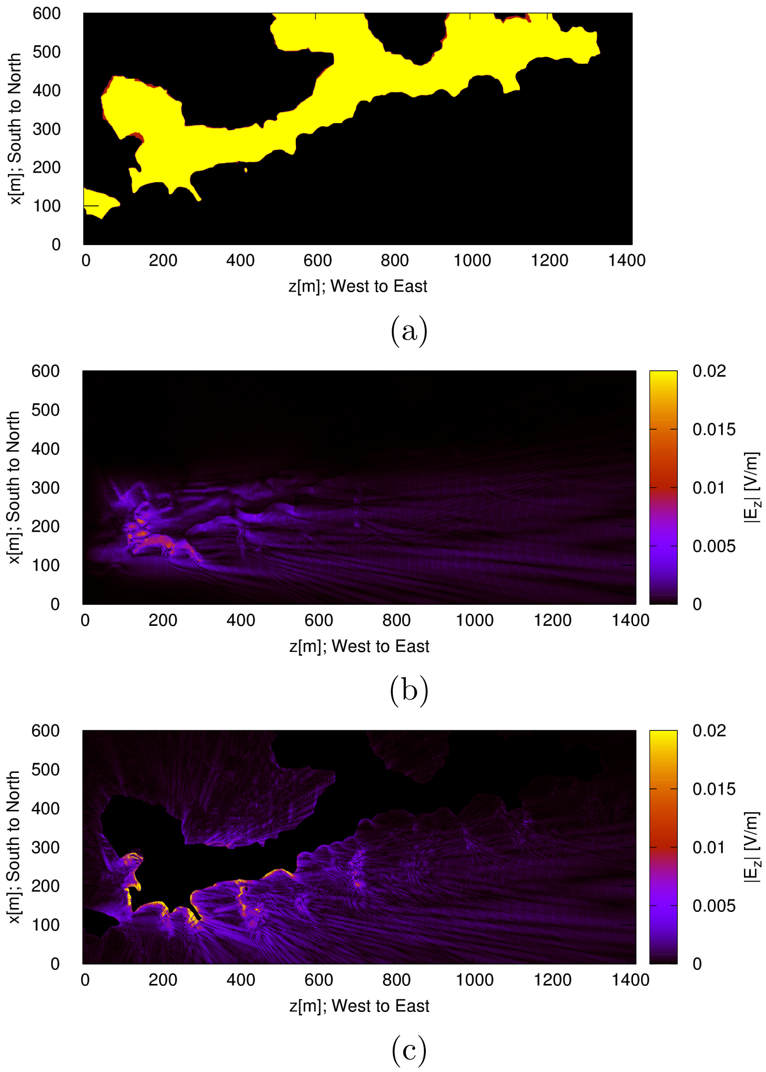

Figure 9. FDTD analysis results of the coastline of Atsumi Peninsula on the horizontal plane at an altitude of 56 m above sea level. The incident wave is of horizontal E_x polarization radiated from the west, and horizontal E_z component is plotted. (a) Horizontal landform on the plane of the field plot, (b) Without surface charge, and (c) With surface charge.

3.3 Japan Sea North Coast of Central Japan

We also consider the radio wave propagation in the coastal region on the Japan-Sea side near the Itoigawa district in Figure 1, where anomalous signals are often observed. As shown in Figure 7, radio wave observation data for Toyama (first slot) and those for Yatsuo (second slot) have typical characteristics of anti-symmetric behavior and simultaneous fluctuation. For more examples, see Supporting Information (Fujii, 2024c) Section 4.2.3. These anomalies are difficult to explain by meteorological and ionospheric phenomena, whereas they can be explained by the anomalous diffraction at electrically charged ground surfaces.

The radio wave path for this district is from Niigata to Toyama, which is approximately 180 km apart along a coastline and beyond the line of sight due to the curvature of the ocean surface. However, there is a landform of a steep mountain in the very vicinity of the Japan Sea, which is in the Itoigawa district that can cause diffraction of the radio wave by the cliff-like landform. Moreover, the radio wave path crosses the Itoigawa-Shizuoka Tectonic Line, along which the stress-induced electric charges may have a relatively high mobility and appear on the nearby ground.

3.3.1 Numerical Analysis Conditions

The mountainous landform has been extracted from the Itoigawa district as shown in Figure 10, and the propagation and diffraction of the radio wave have been analyzed for this region. The size of the analysis region was 650 m from west to east, 300 m from south to north. The height above sea level is 190 m, and below the sea level is tentatively set as 2 m-deep sea water and 2 m-thick sea bottom, which has only little effect on the analysis, so that the total height is 194 m.

The material parameters are the same as in the previous section, $\epsilon_\infty = 6$, $\sigma = 1.0 \times 10^{-3}$ S/m for the ground, and $\epsilon_\infty = 80$, $\sigma = 4.0$ S/m for the seawater. The parameters of the Drude dispersion are $f_p' = 408$ MHz, and $\Gamma = 2\pi \times 10^6$ rad/s for the electrically charged ground. Seawater is always assumed to be a normal non-Drude lossy conductive medium. These are typical analysis conditions used for other cases of anomalous radio wave diffraction by landforms (Fujii, 2013, 2016, 2023b).

The incident wave is chosen to be 70 MHz with the horizontally polarized E_x-component radiated from east to west, from the rectangular source region from $x = 30$ m to 270 m, and from $y = 112.4$ m to 180.3 m, which simulates the actual radio wave path from the broadcast station in Niigata City.

3.3.2 Numerical Results

This analysis region has a large steep mountainous landform, and the steep and rugged slopes are close to the sea, a part of which is shown on the horizontal cross section of the landform in Figure 11(a). Under normal conditions, the radio wave is blocked by the mountainous landform and only a very weak signal reaches the observation point. This is shown in Figure 11(b) and its expansion (c). However, when electric charges are present, the radio wave is diffracted along the slope and propagates around to reach the other side behind the mountain, which appears imperceptibly in Figure 11(d) because the diffracted wave has the same polarization as the incident wave and is dominated by much stronger incident field; the diffracted wave is clearer in the expanded plot in (e). This phenomenon of diffraction allows the horizontally polarized wave to reach the observation site in Toyama.

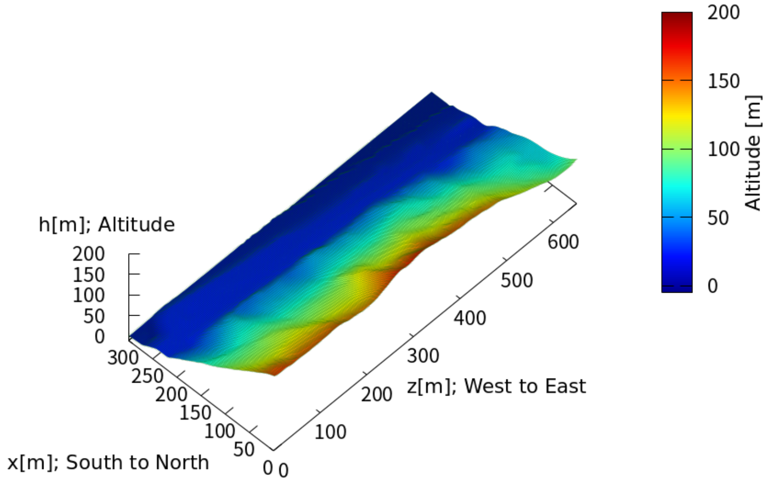

Figure 10. 3D analysis configuration of a coastline along the northern west sea (Japan Sea) side of Japan near Itoigawa City. Altitude h is in the y-direction. the original digital elevation model of approximately 5 m resolution publicized by the Geographical Survey Institute, Japan.

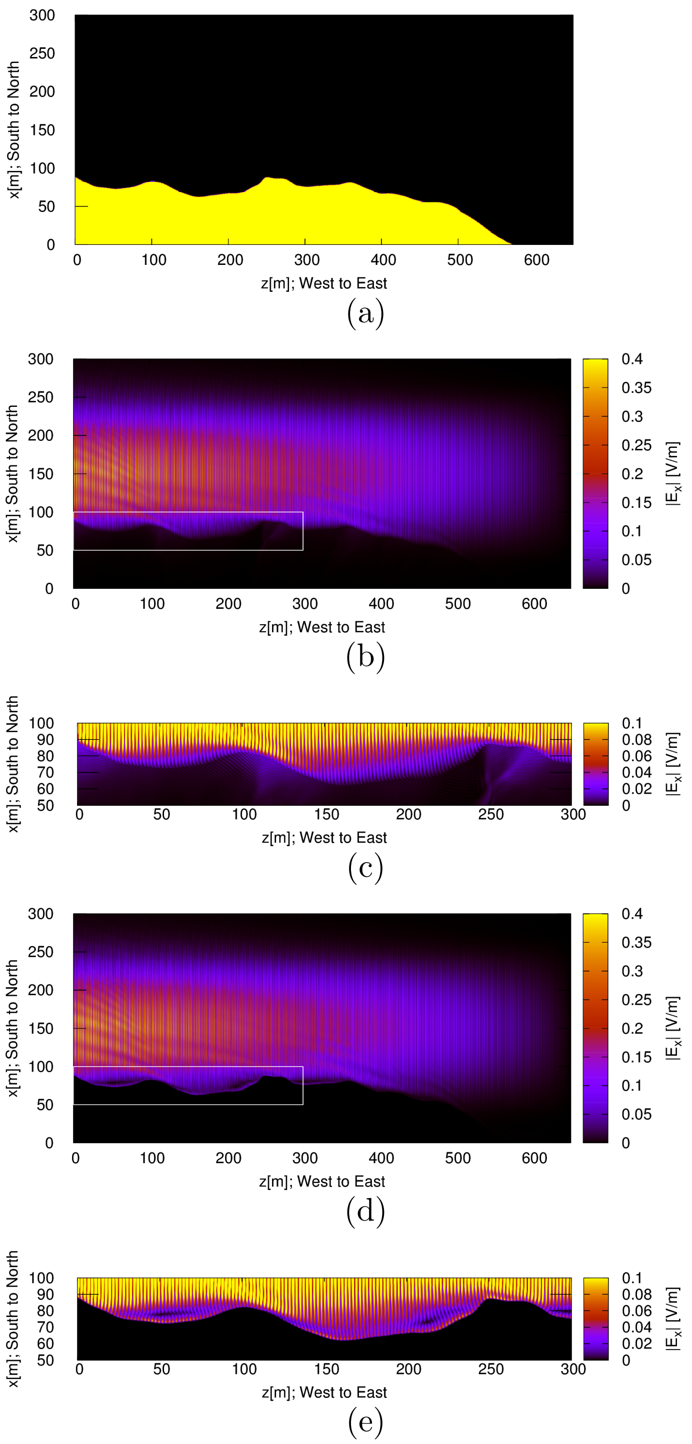

Figure 11. FDTD analysis results of the coastline along the Japan-Sea side of Japan on the horizontal plane at an altitude of 112.4 m above sea level. The incident wave is of horizontal E_x polarization radiated from the east, and the same horizontal E_x-component is plotted. (a) Configuration of the landform on the horizontal plane at an altitude of 112.4 m. (b) Without surface charge, the white rectangular part of the wave propagation is expanded in (c). (c) Without surface charge, the white rectangular part of (b) expanded. (d) With surface charge, the white rectangular part of the wave propagation is expanded in (e). (e) With surface charge, the white rectangular part of (d) expanded.

4 Discussions

We have observed some anomalous radio wave signals before medium and large earthquakes as shown in the previous sections of this paper and in the Supporting Information (Fujii, 2024c). For all the radio waves that show such anomalous signals, we have noticed some common properties regarding the path of the wave: (i) the distance of the radio wave path is slightly beyond the line of sight, and it is not too far and not too close, (ii) there is a possible diffraction point in the middle of the path, for which, if diffraction occurs, the radio wave can reach the observation site, (iii) there is also a major tectonic line nearby, and the radio wave crosses it over or propagates near it. Conversely, if the above conditions are not satisfied, anomalous signals will not appear or will appear only weakly. Therefore, it is reasonable to consider that the anomalous signals were observed as a variation from the normal state of mountain diffraction, which has been well-studied in the past (Barsis & Kirby, 1961).

The above properties are seen in Figure 1 and understood by the coordinates in Table 1; the approximate distances between the broadcast and observation stations are 150 km from Iida to Toyama, 130 km from Tsu to Iwata, and 180 km from Niigata to Toyama, all apparently beyond the line of sight of the radio wave due to the curvature of the Earth and/or the mountains in between. The distance from Shizuoka to Iwata is 68 km, which is relatively shorter than the other distances, but still beyond the line of sight due to the mountains, and the radio wave could be influenced by the nearby Itoigawa-Shizuoka Tectonic Line. The electromagnetic field analyses have confirmed that when the electric charges appear on the ground surface, they interact with radio waves propagating near the ground, and that the interaction causes anomalous diffraction of the radio wave, as suggested also numerically and theoretically (Fujii, 2013, 2016), which supports the above common properties (i) to (iii). The behavior of the interaction varies depending on the landform, e.g., whether it is of mountain or coast.

In mountains, as the surface charges are induced and repel each other, moving toward the peak and accumulating there, the interaction with radio waves continues for a certain period of time depending on the amount of charges generated by the crustal activity. Anomalous signals thus form a rectangular-shaped pulses with a high potential state for the corresponding lifetime of the charges. This agrees with the similar pulse signals observed in the mountainous region in Hokkaido, Japan (Moriya et al., 2010). If the peak of the mountain has at least an area comparable to the wavelength of the radio wave, i.e. only a few meters, then it would act as an antenna and re-radiate waves of vertical polarization, i.e., basically perpendicular to the ground surface near the peak. This scenario is supported by our numerical results.

In contrast, along coasts, surface charges may flow away through the conductive part of the ground or through the seawater, rather than accumulating in one place like the case for a mountain peak. Then the lifetime of such surface charges would be shorter than that on the mountain peaks, and the electric charges would appear and disappear as quickly as they are generated by crustal activity. Thus, the anomalous signals may have a different time variation of the fluctuation compared to that of the rectangular pulses. As briefly mentioned in Sections 3.2 and 3.3, the typical landform of cliffs can cause the anomalous diffraction of the horizontally polarized wave, which is enhanced by the tens of kilometers of coastal landform and then reaches the observation site.

The time period of the possible precursors is years before the earthquakes for our case of the mountainous region of the Japan Alps, while it is only a few days for the case of the coasts of the Atsumi Peninsula and Itoigawa district. This difference is considered to be the difference in the phase of the earthquake; in the preparation phase, which could be a long continuous process before the final failure of the crust, stress is applied to the crusts and elastic potential energy accumulates there; after such a period, immediately before the failure, there could be a foreshock stage, which also varies from a few tens of minutes to a few days, and we can observe a short-term precursor (Dobrovolsky et al., 1989). This scenario varies due to the difference in the crustal properties of the epicentral regions and the rate of stress accumulation on the crust. This will influence the temporal synchrony between the precursors and the occurrence of earthquakes, which can vary greatly depending on the crustal structure and the geology and geography where the precursors are observed. Therefore, the knowledge of the electrical or electromagnetic behavior of the particular site, obtained through long-term observations, would elucidate the typical causality between precursors and earthquakes.

5 Conclusions

Various possible electrical precursors have been detected by electromagnetic wave observation in the central part of Japan. Such anomalous phenomena are generally subtle and vague. However, with our network observation systems and sophisticated noise reduction filters, stable detection of the anomalous signals has been realized. In this paper, the mechanism of the electromagnetic precursors has been proposed and verified by theoretical and numerical analyses of the electromagnetic wave propagation near the surface of the Earth.

We have considered the following particular ground surfaces where we observed possible electromagnetic precursors of earthquakes: (a) a peak of Mt. Okuhotakadake, close to an epicenter in Kamikochi district, (b) a coastline of the Atsumi Peninsula with random cliffs near the Median Tectonic Line, and (c) a coastline of Itoigawa with steep mountain slopes near the Itoigawa-Shizuoka Tectonic Line. From the extensive analysis of these landforms, it has been highly possible that the dominant mechanism of the electromagnetic precursors is the anomalous diffraction by charged ground surfaces; these landforms block the line-of-sight paths of the radio wave propagation, whereas the diffraction of the radio wave by the electric charges on the ground causes significant scattering and re-radiation of the radio wave, which can be detected as precursors at observation sites.

We have demonstrated the stable low-noise observation method, physical mechanism, and numerical analysis of the electromagnetic precursors of earthquakes, which had been extremely controversial and difficult to clarify for a long time. Now, a highly feasible method for monitoring the underground crustal activity and detecting potential earthquake precursors are suggested in terms of where to locate the observation stations and which broadcast stations to choose; i.e., choose the transmitting and observing stations so that the radio wave path is only slightly beyond the line of sight and that the radio wave path crosses a major tectonic line or an expected epicentral zone. Conversely, without fulfilling these conditions, the detection of earthquake precursors would be difficult. We propose the above guidelines to continue monitoring the underground crustal activity, and eventually clarify the correlation property between electromagnetic anomalies and earthquakes.

6 Open Research

Data of earthquakes from the searching service by the Japan Meteorological Agency (JMA) available at `https://www.data.jma.go.jp/svd/eqdb/data/shindo/index.html` (JMA-EQ, n.d.). Precipitation and temperature data from JMA at `https://www.data.jma.go.jp/obd/stats/etrn/` (JMA-Weather, n.d.). Ionograms from the National Institute of Communication Technologies (NICT), Japan at `https://`

wdc.nict.go.jp/Ionosphere/en/archive/summary_viewer/ (NICT, n.d.). Geomagnetic field data from JMA Kakioka Magnetic Observatory, 2013, Kakioka geomagnetic field 1-minute digital data in IAGA-2002 format [dataset], Kakioka Magnetic Observatory Digital Data Service, doi:10.48682/186bd.3f000, available at http://www.kakioka-jma.go.jp/obsdata/metadata (JMA-GM, n.d.).

Supporting Information, including detailed radio wave observation data, is originally available in an institutional repository site at http://www3.u-toyama.ac.jp/densou01/SupportInfo_20240819.pdf, and also in the multiple resource repository site ZENODO for the findable, accessible, interoperable and reusable (FAIR) capability (Fujii, 2024c).

Long-term radio wave data and various environmental data integrated into time-synchronized comparison diagrams are originally available in an institutional repository site at http://www3.u-toyama.ac.jp/densou01/SupportDataSet1_20240819.pdf and http://www3.u-toyama.ac.jp/densou01/SupportDataSet2_20240819.pdf, and also in the multiple resource repository site ZENODO (Fujii, 2024a, 2024b).

Figures were made with Gnuplot version 5.2.8 available under Copyright by T. Williams, and C. Kelley at http://www.gnuplot.info (Williams & Kelley, n.d.).

The map was created using the open-source software QGIS version 3.22.5, available at https://www.qgis.org, and map tiles from the Geographical Survey Institute (GSI), Japan.

acknowledgments

This work is partly supported by the Japan Society for the Promotion of Science (JSPS) KAKENHI Grant Number 21K04059 and 24K07488.

References

Barsis, A., & Kirby, R. (1961, Sep.-Oct.). VHF and UHF signal characteristics observed on a long knife-edge diffraction path. *J. Res. of the National Bureau of Standards - D. Radio Propagation*, *65D*(5), 437-448.

Bleier, T., Dunson, C., Roth, S., Heraud, J., Lira, A., Freund, F., ... Papadopoulos, G. (2013). Earthquake prediction studies: Seismo electromagnetics. In (p. 1-15). Terrapub. (Edited by M. Hayakawa)

Dobrovolsky, I., Gershenzon, N., & Gokhberg, M. (1989). Theory of electrokinetic effects occurring at the final stage in the preparation of a tectonic earthquake. *Phys. Earth Planetary Interiors*, *57*, 144-156.

Dobrovolsky, I., Zubkov, S., & Miachkin, V. (1979). Estimation of the size of earthquake preparation zones. *Pure Appl. Geophys.*, *117*, 1025-1044.

Enomoto, Y., & Hashimoto, H. (1990, Aug.). Emission of charged particles from indentation fracture of rocks. *Nature*, *346*, 641-643.

Enomoto, Y., Tsutsumi, A., Fujinawa, Y., Kasahara, M., & Hashimoto, H. (1997, Dec.). Candidate precursors: Pulse-like geo-electric signals possibly related to recent seismic activity in Japan. *Geophys. J. Int.*, *131*(3), 485-494.

Freund, F. (2000). Time-resolved study of charge generation and propagation in igneous rocks. *J. Geophysical Res., Solid Earth*, *105*(B5), 11001-11019.

Freund, F. (2002). Charge generation and propagation in igneous rocks. *J. of Geodynamics*, *33*, 543-570.

Freund, F. (2011). Pre-earthquake signals: underlying physical processes. *J. of Asian Earth Sciences*, *41*, 383-400.

Fujii, M. (2013, Mar.). Theory of ground surface plasma wave associated with pre-earthquake electrical charges. *Radio Science*, *48*, 122-130.

Fujii, M. (2014, Mar.). Fundamental correction of Mie's scattering theory for the analysis of plasmonic resonance of a metal nanosphere. *Phys. Rev. A*, *89*(3), 033805.

Fujii, M. (2016, Aug.). A new mode of radio wave diffraction via the terrestrial surface plasmon on mountain range. *Radio Science*, *51*, 1396-1412.

Fujii, M. (2021). *Notch filter, Japan patent 6846789* [Japan Patent 6846789].

Fujii, M. (2023a, Aug.). Detection of electromagnetic precursors of earthquakes mediated by the terrestrial ground surface plasma wave. In *URSI GASS 2023* (p. ID.145). Sapporo, Japan. (DOI: 10.46620/URSI-GASS.2023.0145.XHCR4809)

Fujii, M. (2023b, Aug.). Numerical analysis of polarized anomalous electromagnetic diffraction via the ground surface plasma wave associated with earthquakes. In *URSI GASS 2023* (p. ID.464). Sapporo, Japan. (DOI: 10.23919/URSI-GASS57860.2023.10265549)

Fujii, M. (2024a). Supporting data set - 1. (https://doi.org/10.5281/zenodo.12659372)

Fujii, M. (2024b). Supporting data set - 2. (https://doi.org/10.5281/zenodo.12659372)

Fujii, M. (2024c). Supporting information. (https://doi.org/10.5281/zenodo.12659372)

Fujiwara, H., Kamogawa, M., Ikeda, M., Liu, J. Y., Sakata, H., Chen, Y. I., ... Ohtsuki, Y. H. (2004). Atmospheric anomalies observed during earthquake occurrences. *Geophys. Res. Lett.*, *31*, L17110.

Hayakawa, M., Surkov, V. V., Fukumoto, Y., & Yonaiguchi, N. (2007). Characteristics of VHF over-horizon signals possibly related to impending earthquakes and a mechanism of seismo-atmospheric perturbations. *J. of Atmospheric and Solar-Terrestrial Phys.*, *69*, 1057-1062.

JMA-EQ. (n.d.). *Japan meteorological agency seismic intensity database search* [Dataset]. Japan Meteorological Agency. Retrieved from `https://www.data.jma.go.jp/svd/eqdb/data/shindo/index.html`

JMA-GM. (n.d.). *Geomagnetic digital data service* [Dataset]. Japan Meteorological Agency Kakioka Magnetic Observatory. Retrieved from `http://www.kakioka-jma.go.jp/obsdata/metadata`

JMA-Weather. (n.d.). *Japan meteorological agency previous weather data search* [Dataset]. Japan Meteorological Agency. Retrieved from `https://www.data.jma.go.jp/obd/stats/etrn/`

Kamogawa, M., & Ohtsuki, Y. (1999). Plasmon model for origin of earthquake related electromagnetic wave noises. *Proc. Japan Acad.*, *75(B)*, 186-189.

Kittel, C. (1986). *Introduction to solid state physics* (6th ed.). New York: John Wiley and Sons, Inc.

Kushida, Y., & Kushida, R. (1998). On a possibility of earthquake forecast by radio observation in the VHF band. *Riken Rev.*, *19*, 1-13.

Kushida, Y., & Kushida, R. (2002). Possibility of earthquake forecast by radio observations in the VHF band. *J. Atmos. Electricity*, *22*(3), 239-255.

Moriya, T., Mogi, T., & Takada, M. (2010). Anomalous pre-seismic transmission of VHF-band radio waves resulting from large earthquakes, and its statistical relationship to magnitude of impending earthquakes. *Geophysical J. Int.*, *180*, 858-870.

Moriya, T., Mogi, T., Takada, M., & Kasahara, M. (2005, Mar.). Observational research for VHF (FM radio broadcasting waves) scattering waves as a precursor of earthquake occurrence. *Geophysical Bulletin of Hokkaido University*(68), 161-178. (in Japanese)

Moriya, T., Mogi, T., Takada, M., & Yamamoto, I. (2009, Mar.). Observational research for VHF scattering waves prior to earthquakes (II). *Geophysical Bulletin of Hokkaido University*(72), 269-285. (in Japanese)

NICT. (n.d.). *Ionospheric sounding data in Japan, ionogram* [Dataset]. National Institute of Communication Technologies. Retrieved from `https://wdc.nict.go.jp/cgi-bin/ionog/sum_control.cgi`

Pilipenko, V., Shalimov, S., Uyeda, S., & Tanaka, H. (2001). Possible mechanism of the over-horizon reception of FM radio waves during earthquake preparation period. *Proc. Japan Academy*, *77, Ser. B*, 125-130.

Raether, H. (1977). Surface plasma oscillations and their applications. In (Vol. 9, p. 145-261). New York: Academic Press.

Raether, H. (1988). *Surface plasmons on smooth and rough surfaces and on gratings.* Berlin: Springer-Verlag. (p.5)

Rikitake, T., & Yamazaki, Y. (1978). Precursory and coseismic changes in ground resistivity. In *Earthquake precursors, proceedings of the US-Japan seminar on theoretical and experimental investigations of earthquake precursors* (p. 161-173). Tokyo.

Taflove, A. (1995). *Computational electrodynamics: The finite-difference time-domain method.* Artech House Publishers.

Taflove, A., & Hagness, S. C. (2005). Computational electrodynamics: the finite-difference time-domain method. In (3rd ed., p. 361-383). Artech House.

Uyeda, S., Nagao, T., & Kamogawa, M. (2009). Short-term earthquake prediction: current status of seismo-electromagnetics. *Tectonophysics*, *470*, 205-213.

Williams, T., & Kelley, C. (n.d.). *Gnuplot homepage* [Software]. Retrieved from `http://www.gnuplot.info`

Yasuda, Y., Ida, Y., Goto, T., & Hayakawa, M. (2009, Apr.). Interferometric direction finding of over-horizon VHF transmitter signals and natural VHF radio emissions possibly associated with earthquakes. *Radio Science*, *44*(2). (doi:10.1029/2008RS003884)

Yee, K. S. (1966, May). Numerical solution of initial boundary value problems involving Maxwell's equation in isotropic media. *IEEE Trans. Antennas Prop.*, *14*(5), 302-307.

Yoshida, T., M.Nishi, & Mochizuki, K. (2006). Observations of seismic electromagnetic phenomena in VHF band by dual frequency method. *Elec. Eng. Jap.*, *155*(4), 36-44.

References from the Supporting Information

- Y. Kushida and R. Kushida, "On a possibility of earthquake forecast by radio observation in the VHF band", *Riken Rev.*, vol. 19, pp. 1–13, 1998.
- Y. Kushida and R. Kushida, "Possibility of earthquake forecast by radio observations in the VHF band", *J. Atmos. Electricity*, vol. 22, no. 3, pp. 239–255, 2002.
- Y. Kushida, *Earthquake Forecast*, PHP Shinsho, Tokyo, 2012, in Japanese.
- T. Yoshida, M.Nishi, and K. Mochizuki, "Observations of seismic electromagnetic phenomena in VHF band by dual frequency method", *Elec. Eng. Jap.*, vol. 155, no. 4, pp. 36–44, 2006.
- F. Freund, "Charge generation and propagation in igneous rocks", *J. of Geodynamics*, vol. 33, pp. 543–570, 2002.
- T. Rikitake and Y. Yamazaki, "Precursory and coseismic changes in ground resistivity", in *Earthquake Precursors, Proceedings of the US-Japan Seminar on Theoretical and Experimental Investigations of Earthquake Precursors*, Tokyo, 1978, pp. 161–173.
- M. Fujii, "Fundamental correction of Mie's scattering theory for the analysis of plasmonic resonance of a metal nanosphere", *Phys. Rev. A*, vol. 89, no. 3, pp. 033805, Mar. 2014.
- M. Fujii, "A new mode of radio wave diffraction via the terrestrial surface plasmon on mountain range", *Radio Science*, vol. 51, pp. 1396–1412, Aug. 2016.
- K. Hosokawa, J. Sakai, S. Saito, T. Tsugawa, M. Nishioka, and M. Ishii, "A monitoring network for anomalous propagation of aeronautical VHF radio waves due to sporadic E in Japan", *Earth Planets Space*, vol. 72, pp. 88, July 2020, https://doi.org/10.1186/s40623-020-01216-z.
- A. Taflove and S. C. Hagness, *Computational electrodynamics: the finite-difference time-domain method*, chapter 9, pp. 361–383, Artech House, 3rd edition, 2005.
- M. Fujii, "Theory of ground surface plasma wave associated with pre-earthquake electrical charges", *Radio Science*, vol. 48, pp. 122–130, Mar. 2013.
- M. Kamogawa and Y. Ohtsuki, "Plasmon model for origin of earthquake related electromagnetic wave noises", *Proc. Japan Acad.*, vol. 75(B), pp. 186–189, 1999.
- F. Freund, "Time-resolved study of charge generation and propagation in igneous rocks", *J. Geophysical Res., Solid Earth*, vol. 105, no. B5, pp. 11001–11019, 2000.
- J. Scoville, J. Sornette, and F. Freund, "Paradox of peroxy defects and positive holes in rocks Part II: Outflow of electric currents from stressed rocks", *J. of Asian Earth Sciences*, vol. 114-2, pp. 338–351, Dec. 2015.
- F. Freund, *Triboluminescence - Theory, Synthesis, and Applications*, pp. 17–37, Springer, 2016.
- A. Agrawal, S. H. Cho, O. Zandi, S. Ghosh, R. W. Johns, and D. J. Milliron, "Localized surface plasmon resonance in semiconductor nanocrystals", *Chem. Rev.*, vol. 118, pp. 3121–3207, 2018.
- C. Kittel, *Introduction to solid state physics*, John Wiley and Sons, Inc., New York, 6th edition, 1986.
- H. Raether, *Surface plasmons on smooth and rough surfaces and on gratings*, Springer-Verlag, Berlin, 1988, p.5.